Excerpt from the Proceedings of the 2011 COMSOL Conference in Boston

Deformation of biconcave Red Blood Cell in the Dual-beam Optical Tweezers

Lingyao Yu[1], Yi He[2], Arthur Chiou[2] and Yunlong Sheng[1,*]

1 Center of Optics, Photonics and Lasers, Dept. of Physics, University Laval, Quebec, Canada

[2] Institute of Biophotonics Engineering, National Yang-Ming University, Taipei, Taiwan

*sheng@phy.ulaval.ca; phone 1 418 656-2131 3908; fax 1 418 656-2623; fourier.phy.ulaval.ca/~sheng

Keywords: Optical tweezers; Optical manipulation; Cell mechanics; Red Blood Cells; Mechanics of Membrane; Elastic deformation; Finite Element methods; Multi-physics.

ABSTRACT

Red Blood Cell (RBC) suspended in aquatic buffer is trapped and deformed by the dual-beam optical tweezers in order to measure the elasticity of the cell's membrane. In this experiment, the RBCs were in the natural form of biconcave disc shape. We modeled a highly focused trapping beam of numerical aperture NA=1.25 as a spherical wave with Gaussian intensity distribution in a stationary study mode, and built the background optical field by adding two such waves shifted in a lateral direction. The perfect matched layers (PML) were selected to define the computation domain. The 3D radiation stress distribution on the biconcave RBC surface was computed by Comsol multi-physics Radio Frequency Module™ via the Maxwell stress tensor, and the 3D deformation of the biconcave RBC was then computed with the elastic membrane theory with Comsol Structure Mechanics Module™. The linear elastic material model with nearly incompressible material and geometric nonlinearity were set up to study large deformation of the cell. The two modules were fully coupled and used the moving mash to compute in a recursive process the electromagnetic field and the radiation stress distribution on the deformed RBC of any geometric shape and its consequent deformation until the final equilibrium state. The computed deformations in the background field with different beam separations and laser powers can fit to the experimental data in order to determine the Young's elasticity module of the cell membrane.

INTRODUCTION

Optical tweezers has been demonstrated to be able to conveniently manipulate the single living cell as a noninvasive trapping method [1-3]. The trapping force in the optical tweezers can be quantitatively calibrated to measure bio-molecular interactions [4,5], and to study the visco-elastic properties of an isolated cell using various multiple-trap optical tweezers. Two glass or polystyrene beads attached to a human red blood cell (RBC) are manipulated by two focused laser beams to stretch the cell and study its mechanical characteristics [6, 7]. The multiple-trap optical tweezers have been also applied directly to the cells [8-10] without physical contact. Bronkhorst et al used triple-traps to bend the discotic RBCs and measure the recovery time of a deformed cell [11]. Liao et al used a

jumping beam optical tweezers to measure the RBC's elongation as a function of the beam jumping amplitude with the trapping beam controlled by an acousto-optics modulator. They qualitatively explained the experimental results with the two-dimensional (2D) stress distribution on the RBC discotic equator [12]. Rencourt-Grenier et al computed 3D dynamic deformation of a spherical RBC in a dual-trap optical tweezers using the geometrical ray-tracing approach to calculate the radiation stress distribution on the cell's membrane and the Comsol Structure Mechanics Module™ to calculate the cell's deformation [13,14], and fit the data to experimental results. The Comsol™ modules allowed computing redistribution of the stress as the cell was deformed gradually and the consequent new deformation of the cell. In this work [13-14], however, the RBC specimen has had to be swollen to the spherical shape from its natural biconcave shape by the osmotic pressure. In addition, the geometrical optics ray tracing can only compute the stress distribution on a spherical cell. When the cell is deformed from the spherical shape the geometrical optics approach is approximate.

In this paper, we present a model of the biconcave RBC deformation in the dual-beam optical tweezers. We benefit from advantages of the COMSOL multiphysics™ to make two important advances in our computation. First, the COMSOL Radio Frequency Module™ has been used to compute the optical radiation stress distribution on the cell's membrane of arbitrary shape via the Maxwell stress tensor in stead of the geometrical optics ray tracing approach. Second, the COMSOL Multiphysics ™ allowed to import the solid of the biconcave-shape RBC. Compared with the experimental results, our simulation is able to determine the share modulus of the membrane of a natural biconcave-shaped RBC.

THEORETICAL MODEL

The geometrical shape of a normal healthy RBC in the ideal situation is determined by the average geometry and is given by [1,2]

$$x = \pm D_0 \sqrt{1 - \frac{4\left(y^2 + z^2\right)}{D_0}} \left[c_0 + c_1 \frac{y^2 + z^2}{D_0^2} + c_2 \frac{\left(y^2 + z^2\right)^2}{D_0^4} \right] \tag{1}$$

where the diameter of the discotic in the *x*-*z* plane D_0 is set to 7.8μm and other parameters are set to be $(c_0, c_1, c_2)=(0.05179025, 2.002558, -4.491048)$ as illustrated in Fig. 1.

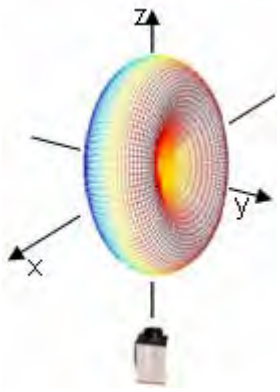

Fig. 1 Biconcave-shaped RBC with the equator diameter D_0=7.8 μm in an optical tweezers. Two laser beams are parallel to the z-axis shifted by $S/2$ in $\pm x$ directions and focused on the *x*-axis

To compute the stress distribution on the surface of the biconcave RBC, the electromagnetic background field of the dual-trap optical tweezers was first established via the electromagnetic waves module of COMSOL mulitiphysics with the stationary study mode. In order to simulate the dual-trap optical tweezers, two trapping beams were introduced. Each beam was modeled as a radial polarized spherical wave with Gaussian intensity distribution in the transversal sections, propagating along the +*z* axis and focused at (*x*= ±*S*/2, *y*=*z*=0), respectively. The electrical field had the components in *x*, *y*, and *z* directions determined by the radial polarization, and the complex amplitude of the electrical intensity related to the intensity *I* of the optical beam as

$$|E|^2 = 2I\eta \qquad with \quad \eta = \eta_0 / n \quad and \quad \eta_0 = 120\pi \tag{2}$$

where η_0 is the impedance in the vacuum, *n* is the index of refraction, the optical intensity *I* is related to the beam power *P* as

$$P = \frac{1}{2} I_0 \left(\pi W_0^2\right) \tag{3}$$

and

$$I = I_0 \left[\frac{W_0}{W(z)}\right]^2 \exp\left[-\frac{2(x^2+y^2)}{W^2(z)}\right]$$

where I_0 is the optical intensity at the peak point in the Gaussian intensity distribution, $W(z) = W_0[1+(z/z_0)^2]^{1/2}$ is the radius of the cross section of the Gaussian beam and $W_0 = \lambda/\pi \tan\left(\sin^{-1}\left(NA/n\right)\right)$ is the waist radius with the Rayleigh range $z_0 = \pi W_0^2/\lambda$. The numerical aperture of the beam *NA*= 1.25. The laser power *P* was set to 10 mW at the center wavelength 1.06 μm. The electric intensity E_{b1} and E_{b2} of the two beams in the background beams with the separation *S* are expressed by

$$E_{b1} = \frac{\sqrt{240nP}}{W(z)} \exp\left(-\frac{(x-S/2)^2+y^2}{W(z)^2}\right) \exp\left[\mathrm{j}\frac{2\pi}{\lambda}[(x-S/2)^2+y^2+z^2]\right] \tag{4}$$

$$E_{b2} = \frac{\sqrt{240nP}}{W(z)} \exp\left(-\frac{(x+S/2)^2+y^2}{W(z)^2}\right) \exp\left[\mathrm{j}\frac{2\pi}{\lambda}[(x+S/2)^2+y^2+z^2]\right] \tag{5}$$

The values of the refractive index n_2 in the cell and n_1 in the buffer were set to be 1.378 and 1.335, respectively. The perfect matched layers (PML) were selected as the additional domain which absorbs the incident radiation without producing reflections. In the PML, the material properties were with the electric conductivity equal to zero (S/m), the relative permittivity ε_r=1.378^2 and the relative permeability μ_r=1.

The two identical beams separated by *S* were set as the background field. The components of the total fields (E_{b1}+E_{b2}) in the *x*, *y*, and *z* directions are added in the complex amplitude and thus generate interference fringes. This interference undesirable for optical trapping does exist physically in the dual-beam optical tweezers, but does not exist in the jumping optical tweezers, where a single laser beam is jumped over a distance *S* by using the acousto-optic modulator. To avoid the weak interference between the two beams in our simulation, we computed the radiation stress distribution on the cell

surface due to each single beam, E_{b1} and E_{b2} with the RF modules, and then added the stress distributions on the cell surface, resulting from the two beams as the total stress.

After introducing the biconcave-shaped RBC and the trapping beam in the background, the COMSOL RF module™ is able to solve the electromagnetic field in the space domain. The radiation stress on the RBC surface was computed from the electrical field intensity via the Maxwell stress tensor. After some mathematical manipulations from the Maxwell stress tensor the radiation stress $\vec{\sigma}$ in the unit of N/m^2 can be expressed as

$$\vec{\sigma} = \frac{\varepsilon_0}{2}\left(n_1^2 - n_2^2\right)\left(\left(\frac{n_1^2}{n_2^2}\right)E_n^2 + E_t^2\right)\vec{n} \tag{6}$$

where the tangent component $\left|\vec{E}_t\right| = \left|\vec{E} \times \vec{n}\right|$ and the normal component $\left|E_n\right| = \left|\vec{E} \cdot \vec{n}\right|$. In addition, we can demonstrate that the radiation stress is always normal to the interface. The total force F on the cell can be calculated by the surface integration of the stress σ. Figure 2 shows the 3D normalized stress distribution on the surface of the cell as a function of the beam separation applied to the biconcave-shaped RBC. In order to compare the computational results with the experimental data, the diameter of the cell disk equator has been scaled to 7.5 μm by the scale function in COMSOL geometry interface.

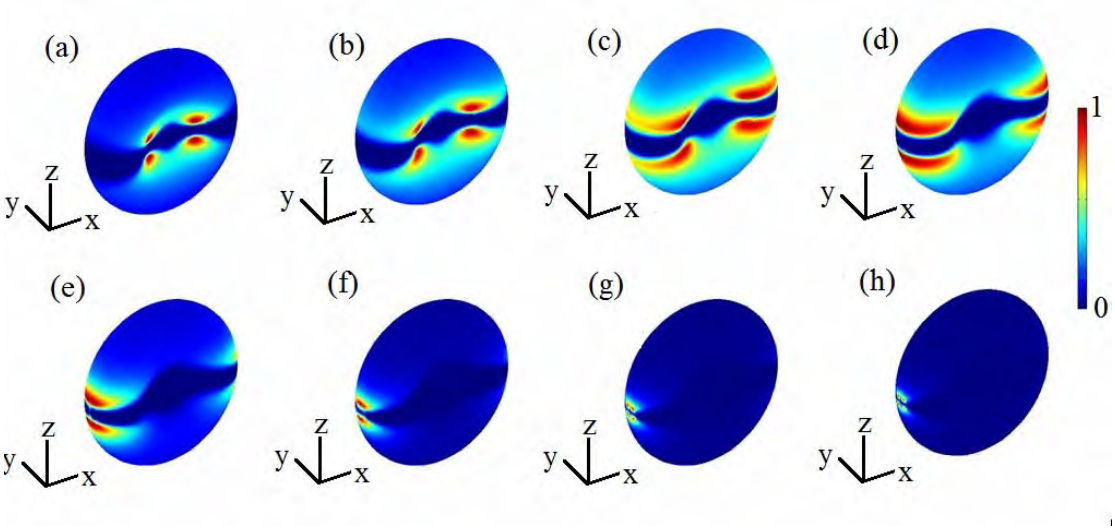

Fig. 2. (a)-(h) 3D normalized stress distribution on the surface of a biconcave-shaped RBC with the beam separation S= 3.1, 3.8, 4.5, 5.2, 5.9, 6.6, 7.0 and 7.3 μm computed by the COMSOL RF module. The trapping beam is radial polarized spherical waves with the Gaussian intensity distribution along the +z axis, focused at (x=±S/2, y=z=0), NA=1.25, and cell disk equator diameter 7.5 μm.

With the computed stress distributions on the surface of the cell, we applied the linear elastic material model to the RBC membrane and nearly incompressible material model to the membrane of the RBC to compute its deformation. Assume that the continuum medium of the cell membrane keeps a content volume we set the Poisson's ratio of the RBC's membrane to 0.4999. The Young's Modulus was set according to the experimental data and to 100N/m^2 for the final fitting. The COMSOL solid mechanics module was used to compute the deformation of the RBC. As the deformation of RBC was the most important phenomenon about which we primarily cared in the simulation, the shift of the whole cell produced by the non-zero total force in the background field was neglected in this simulation. Thus, six poles of intersection of the cell surface with the x, y, and z axes were set,

respectively, which were constrained to move only on the corresponding axis, such that the cell can be only deformed symmetrically with respect to the axes, but not be free to shift in the space.

The RF™ and Structure Mechanics™ modules were fully coupled, and the moving mesh was used in a recursive process, in which the electromagnetic field and the redistribution of the radiation stress on the deformed RBC and its consequent deformation were computed in iterations until the final deformation of the cell in an equilibrium state was achieved. To solve this multiphysics problem, we launched the stationary solution with the SPOOLES solver as well as the damped version of Newton's method in COMSOL with the finite element method (FEM). Figure 3 shows the 3D normalized displacements on the surface of the deformed RBC as a function of the beam separations *S*, which are ready to fit to the experimental results.

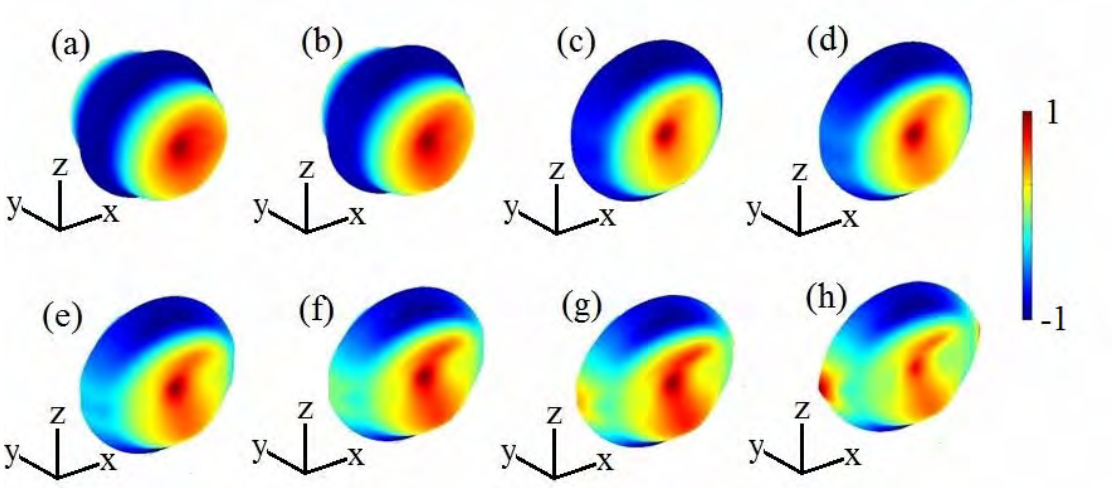

Figure 3 (a)-(h) 3D normalized deformation of the RBC at the beam separation *S*=3.1, 3.8, 4.5, 5.2, 5.9, 6.6, 7.0 and 7.3 μm. The color encodes the displacements of the RBC's surface, which are positive (outward from the RBC) or negative (inward to the RBC)

EXPERIMENTAL RESULTS

The jumping beam optical tweezers setup has been described in literature [12]. The experimental results of the deformed RBC as a function of the beam jumping distance are shown in Fig. 4a. Only the cell's deformation along the *x* axis can be monitored and observed in this experiment. Fig. 4b shows the FEM computational results of the *x*-axial elongation of the RBC as a function of the beam separation *S*, as well as the experimental results for comparison. The fitting parameters depend on the product of the cell's membrane Young's modulus and the membrane thickness *Eh* and the cell's original diameter D_0. In this fitting, the parameters were *Eh*=3.7 μN/m and D_0=7.5μm.

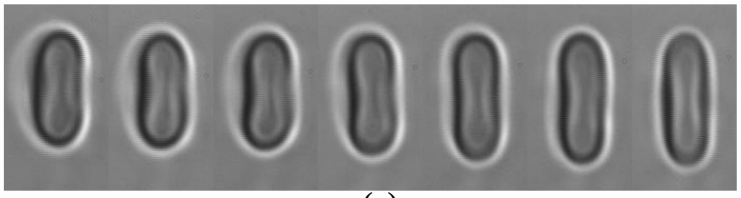

(a)

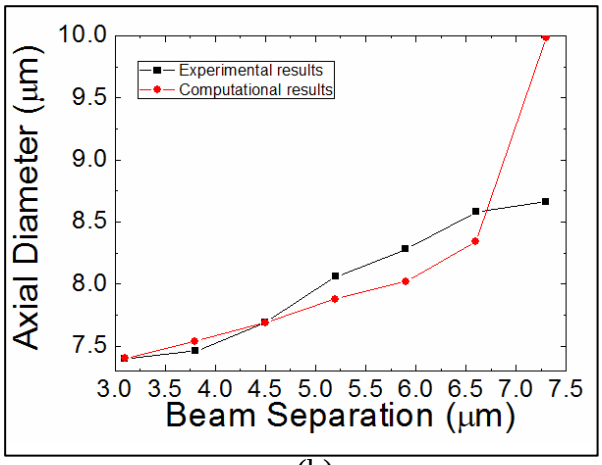

(b)

Figure 4 (a): Images of a trapped and stretched RBC with the beam separations D=3.1, 3.8, 4.5, 5.2, 5.9, 6.6 and 7.3 μm (from left to right); (b): computational results using COMSOL multiphysics modules with FEM versus experimental data.

From the computation results shown in Figs. 2 and 3 we see that when the beam jumping distance is small, S < 4.5 μm, the stress generated by the two beams of high *NA* are mostly concentrated in the internal concaved region of the RBC. In this case, the cell membrane is deformed mostly in the *y*-direction perpendicular to the cell discotic. In the observation along the z-axis the cell could not be seen elongated but a little shorten in the *x*-direction. This is in agreement with the experiments. When the beam jumping distance increases the stress distribution becomes more concentrated in the outer region of the cell biconcaved shape, and leads to cell's elongation. When the jumping distance S =7.3 μm the excessive cell elongation obtained by the calculation is due to the two highly concentrated stress spots on the cell, as shown in Figs. 2h and 3h, which has not been observed in the experiments. In fact, in this case the trapping beam focus is on the edges of the cell and the trapping is not stable.

CONCLUSION

We have computed the deformation of a red blood cell in its natural biconcave-shape in the jumping beam optical tweezers. We have benefited from advantages of the COMSOL multiphysics™ to make two important advances with respect to our previous computation [13]. First, the Radio Frequency Module™ is used to replace the geometrical optics ray tracing approach to compute the optical field and the radiation pressure distribution. Second, the natural biconcave-shape of the RBC is used instead of the spherical shape of the cell in the previous computation. The theoretical calculation was fit to the experimental data in terms of the axial elongation of the cell as a function of the beam separation and resulted in the measured Young's modulus *Eh*=100 N/m. In the next step we shall let the cell floating in the background optical field in order to determine its equilibrium position in the optical trap and compute the cell deformation at this position.

References

1. A. Ashkin, J. M. Dziedzic, and T. Yamane, "Optical trapping and manipulation of single cells using infrared laser beams," Nature **330**(6150), 769–771 (1987).

2. S. M. Block, “Making light work with optical tweezers,” Nature **360** (6403), 493–495 (1992).

3. J. Guck, R. Ananthakrishnan, H. Mahmood, T. J. Moon, C. C. Cunningham, and J. Käs, “The optical stretcher: a novel laser tool to micromanipulate cells,” Biophys. J. **81**(2), 767–784 (2001).

4. M. J. Lang, C. L. Asbury, J. W. Shaevitz, and S. M. Block, “An automated two-dimensional optical force clamp for single molecule studies,” Biophys. J. **83**, 491-501 (2002).

5. S. L. Liu, A. Karmenyan, M. T. Wei, C. C, Huang, C, H, Lin, and A, Chiou, “Optical forced oscillation for the study of lectin-glycoprotein interaction at the cellular membrane of a Chinese hamster ovary cell,” Opt. Express **15**, 2713-2723 (2007).

6. M. Dao, C. T. Lim, and S. Suresh, “Mechanics of the human red blood cell deformed by optical tweezers,” J. Mech. Phys. Solids **51**(11-12), 2259–2280 (2003).

7. S. Hénon, G. Lenormand, A. Richert, and F. Gallet, “A new determination of the shear modulus of the human erythrocyte membrane using optical tweezers,” Biophys. J. **76**(2), 1145–1151 (1999).

8. P. J. H. Bronkhorst, G. J. Streekstra, J. Grimbergen, E. J. Nijhof, J. J. Sixma, and G. J. Brakenhoff, “A new method to study shape recovery of red blood cells using multiple optical trapping,” Biophys. J. **69** (5), 1666–1673 (1995).

9. W. G. Lee, H. Bang, J. Park, S. Chung, K. Cho, C. Chung, D.-C. Han, and J. K. Chang, “Combined microchannel-type erythrocyte deformability test with optical tweezers,” *Proc. of SPIE.* **6088**, 608813–1-12, (2006).

10. P. B. Bareil, Y. Sheng, and A. Chiou, “Local scattering stress distribution on surface of a spherical cell in optical stretcher,” Opt. Express **14**(25), 12503 (2006).

11. P. J. H. Bronkhorst, G. J. Streekstra, J. Grimbergen, E. J. Nijhof, J. J. Sixma, and G. J. Brakenhoff, “A new method to study shape recovery of red blood cells using multiple optical trapping,” Biophys. J. **69**(5), 1666–1673 (1995).

12. G. B. Liao, P. B. Bareil, Y. Sheng, and A. Chiou, “One-dimensional jumping optical tweezers for optical stretching of bi-concave human red blood cells,” Opt. Express **16**(3), 1996–2004 (2008).

13. Y. Sheng at el, “Dynamic deformation of soft particle in dual-trap optical tweezers”, COMSOL Conference Boston (2010)

14. S. R. Grenier, M. Wei, J. Bai, A. Chiou, P. Bareil, P. Duval, and Y. Sheng, ”Dynamic deformation of red blood cell in dual-trap optical tweezers ” Opt. Express **18**(10), 10462–10472 (2010).